J. Fluid Mech. (2008), *vol.* 597, *pp.* 395–414.
doi:10.1017/S0022112007000018 Printed in the United Kingdom

Interaction between two quasi-geostrophic vortices of unequal potential vorticity

ERSIN ÖZUĞURLU[1,2], JEAN N. REINAUD[1]† AND DAVID G. DRITSCHEL[1]

[1]Mathematical Institute, University of St Andrews, St Andrews, KY16 9SS, UK
[2]Faculty of Arts and Science, Bahcesehir University, Besiktas 34100, Istanbul, Turkey

(Received 10 December 2006 and in revised form 22 October 2007)

In this paper we systematically investigate strong interactions between two like-signed quasi-geostrophic vortices containing different uniform potential vorticity. The interaction depends on six parameters: the potential vorticity ratio between the two vortices, their volume ratio, their individual height-to-width aspect ratio, their vertical offset, and their horizontal separation distance. We first determine the conditions under which a strong interaction may occur. To that end, we calculate equilibrium states using an asymptotic approach which models the vortices as ellipsoids and we additionally assess their linear stability. It is found that vortices having similar potential vorticity interact strongly (e.g. merge) at closer separation distances than do vortices with a dissimilar potential vorticity. This implies that interactions between vortices having significantly different potential vorticity may be more destructive, for a given separation distance. This is confirmed by investigating the nonlinear evolution of the vortices over a subset of the full parameter space, solving the full dynamical quasi-geostrophic equations. Many forms of interaction occur, but merger or partial merger (where the largest vortex grows in volume) is mostly observed for interactions between vortices of similar potential vorticity.

1. Introduction

The Earth's atmosphere and oceans are complex fluid systems whose characteristic horizontal scales of motion span a broad spectrum up to the order of thousands of kilometres in the atmosphere and hundreds of kilometres in the oceans. Atmospheric and oceanic flows are also strongly affected by the Earth's rotation and the largely stable density stratification.

In recent years, much attention has been paid to the study of coherent vortical structures, or 'vortices', in geophysical flows. Coherent vortices are common features in the atmosphere and oceans (see Garrett 2000). For example, Ebbesmayer *et al.* (1986) extrapolated from field measurements that between 1000 to 10 000 vortices exist in the surface layers of the North Atlantic alone. Vortices can be identified as compact volumes of anomalous potential vorticity (PV), and the dynamics of the atmosphere and the oceans is mainly driven by the interaction between these vortices and larger-scale jets: sharp gradients of PV. In the absence of diabatic effects and viscous diffusion (negligible for the time and space scales considered here), PV is materially conserved, and provides a convenient dynamical tracer for identifying

† Author to whom correspondence should be addressed.

vortices. The simplest approximate model which describes the evolution of rapidly rotating, stably stratified flows is the 'quasi-geostrophic' (QG) model (cf. Gill 1982 for a complete discussion). In the QG model the PV distribution alone determines all other fields.

Early studies of vortex interactions focused on two-dimensional or barotropic vortices. Such vortex interactions have been extensively studied both for co-rotating and counter-rotating vortices (see Dritschel 1995, and references therein). One of the main results of these studies is the identification of a critical distance, below which two equal-vorticity patches strongly interact, e.g. by merging partially or completely, or by straining out one vortex either partially or completely (Dritschel & Waugh 1992).

In three-dimensional QG flows, vortex interactions have been studied by Dritschel & de la Torre Juárez (1996), von Hardenberg *et al.* (2000), Dritschel (2002), Reinaud & Dritschel (2002) and others, using the QG model. These studies considered the simplest situations in which some symmetries were present in the initial conditions. The full parameter space is too large to be thoroughly investigated. As a result, we still know little about QG vortex interactions in general.

Dritschel, Reinaud & McKiver (2004) developed a greatly simplified model of QG dynamics which represents vortices as uniform-PV ellipsoids and filters higher-order non-ellipsoidal deformations. This ellipsoidal vortex model (ELM) takes full account of the ellipsoid-preserving part of the interactions between vortices. The ELM builds on earlier models for a single ellipsoid developed by Meacham (1992) Meacham *et al.* (1994, 1997), and in particular McKiver & Dritschel (2003), who reformulated the single-vortex model using a matrix description. A multi-vortex ellipsoidal model was previously developed by Miyazaki, Furuichi & Takahashi (2001) and applied to study interacting vortices. However, this model was based on a moment-expansion approximation of vortex interactions, and this model proves inaccurate compared to the ELM, particularly for close interactions (Dritschel *et al.* 2004).

Reinaud & Dritschel (2005) adapted the ELM to determine equilibrium states and to assess the linear stability of two interacting vortices. Although the stability analysis is restricted to 'ellipsoidal modes', comparison with a stability analysis based on the full QG equations showed that this approach is able to capture the first unstable mode for co-rotating vortices. In other words, the first unstable mode is consistent with ellipsoidal deformations. Reinaud & Dritschel (2005) also stressed that the study of symmetric vortex configurations can be highly misleading. They demonstrated that even the slightest break in symmetry can have profound consequences, leading for instance to vortex merger from greater separation distances than occurs between perfectly symmetric vortices. In short, one should avoid imposing symmetry, which does not typify general vortex interactions.

For simplicity, Reinaud & Dritschel (2005) focused on equal-PV vortices (with a non-zero vertical offset to avoid symmetry). This is nevertheless an important case, as we shall see below. The ELM can also be used for vortices having different PV, at the price of enlarging the parameter space yet further. Here we do this in order to understand how differences in PV affect vortex interactions.

In this paper, we focus on vortices having height-to-width aspect ratios in the range 0.6 to 1.2 (after stretching z by the buoyancy-Coriolis frequency ratio). This range covers a large proportion of the vortices found in fully developed QG turbulence (Reinaud, Dritschel & Koudella 2003). Moreover, we consider a broad range of vertical offsets between the two vortices, together with a variety of PV ratios and volume ratios.

A large subset of the marginally unstable equilibria are then taken as initial conditions for fully-nonlinear QG simulations carried out with the 'contour-advective semi-Lagrangian' (CASL) algorithm (Dritschel & Ambaum 1997). We focus on how these interactions modify the vortex properties such as the volume, strength and the number of major structures produced. Bambrey, Reinaud & Dritschel (2007) conducted an investigation of vortex interactions in a large parameter space for two equal-PV vortices. Based on ensemble averages of the outcome of the interactions, the authors confirmed a net inverse energy cascade like that observed in QG turbulence. The energy cascade is dominated by the formation of relatively few large vortices. On the other hand, a direct enstrophy cascade occurs via the formation of a great number of small vortices over a wide range of scales. Moreover, it was found that 'complete merger' in which two vortices form a single large vortex with little debris is extremely rare. In most cases, merger is only partial with much debris and one or more secondary vortices. Hence, generally, vortex interactions contribute more weakly than one might expect to the energy and (consequently) enstrophy cascades. In this paper, we consider various PV ratios, and for a given PV ratio between the two vortices, we conduct a similar investigation to complement the results of Bambrey *et al.* (2007), on a smaller parameter space per PV ratio.

The paper is organized as follows. In § 2, we give a short introduction to the QG model and outline the numerical methods. Section 3 describes equilibrium solutions and their linear stability. The nonlinear interaction of two vortices is considered in § 4. Some conclusions and perspectives for future work are offered in § 5.

2. Formulation of the problem

2.1. *The QG approximation*

The QG model can be obtained by an asymptotic expansion of Euler's equations with $H/L \ll 1$, where H and L are, respectively, the vertical and horizontal characteristic length scales, and $Fr^2 \ll Ro \ll 1$, where $Fr = U/NH$ is the Froude number, and $Ro = U/fL$ is the Rossby number. Here, U is the horizontal velocity scale, N is the buoyancy frequency and f is the Coriolis frequency (see e.g. Gill 1982 for a complete discussion). In this context, the fluid motion is fully determined by the slow evolution of a scalar field, the potential vorticity anomaly q.

In an adiabatic dissipationless fluid, q is materially conserved i.e.

$$\frac{\mathrm{D}q}{\mathrm{D}t} \equiv \frac{\partial q}{\partial t} + \boldsymbol{u} \cdot \nabla q = 0, \tag{2.1}$$

where $\boldsymbol{u}$ is the two-dimensional advecting velocity field, tangent to iso-density surfaces, which can be deduced from a scalar streamfunction ψ

$$\boldsymbol{u}(\boldsymbol{x}, t) = \left(-\frac{\partial \psi}{\partial y}, \frac{\partial \psi}{\partial x}, 0 \right). \tag{2.2}$$

For the sake of simplicity, and following many previous studies, we take N and f both constant. Although N varies in the real ocean and across the tropopause, taking N constant over the height of the vortices considered greatly simplifies the problem, without fundamentally altering, we believe, the characteristics of vortex interactions. Then, by stretching the vertical direction z by N/f, the streamfunction ψ may be determined from the PV distribution $q(x, y, z, t)$ by inverting Laplace's operator:

$$\Delta \psi = q(x, y, z, t). \tag{2.3}$$

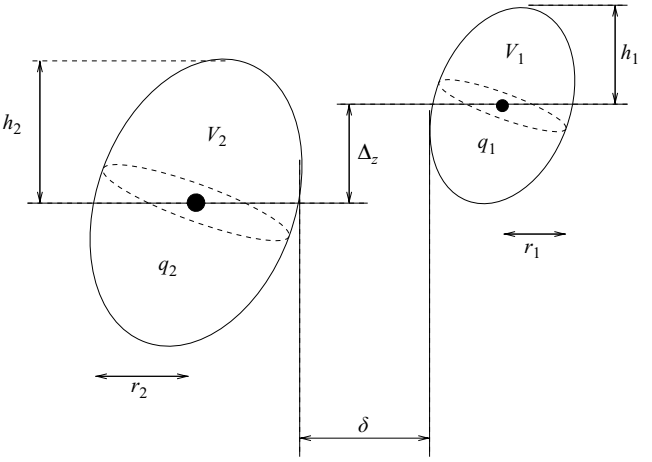

FIGURE 1. Geometry of a vortex equilibrium configuration.

2.2. *Numerical procedures*

We seek the critical distance between two co-rotating vortices in mutual equilibrium within which the equilibrium is unstable. This instability always triggers the strong interaction between the two vortices, based on extensive experience. The problem at hand depends on five parameters: the PV ratio, volume ratio, two height-to-width aspect ratios, and the vertical offset between the two vortices. For each set of parameter values, we decrease the horizontal gap δ between the innermost edges of the vortices (see figure 1) until we reach marginal stability at the 'critical gap' δ_c. Below this, for $\delta < \delta_c$, the equilibria are unstable. We thus find an entire family of vortex equilibria to determine δ_c.

Because of the size of the parameter space, computing the equilibrium states and their linear stability using the full QG equations is not viable. Following Reinaud & Dritschel (2005), we use the ELM as an approximate but highly efficient alternative. Vortices are modelled as ellipsoids and higher-order non-ellipsoidal deformations are filtered. Although approximate, the ELM proves surprisingly accurate for close separation distances (see Dritschel *et al.* 2004; Reinaud & Dritschel 2005). A brief outline of the ELM is provided below. The ELM is a Hamiltonian system for the motion and the deformation of interacting PV ellipsoids. For the ith ellipsoid, the governing equations read

$$\frac{\mathrm{d}\boldsymbol{X}_i}{\mathrm{d}t} = -\frac{1}{\kappa_i}\mathscr{L}\frac{\partial H}{\partial \boldsymbol{X}_i}, \tag{2.4}$$

and

$$\frac{\mathrm{d}\mathscr{B}_i}{\mathrm{d}t} = \mathscr{S}_i\mathscr{B}_i + \mathscr{B}_i\mathscr{S}_i^T, \tag{2.5}$$

$$\mathscr{S}_i = -\frac{10}{\kappa_i}\mathscr{L}\frac{\partial H}{\partial \mathscr{B}_i}, \tag{2.6}$$

where $\boldsymbol{X}_i = (X_i, Y_i, Z_i)$ is the vortex centroid position, and $\mathscr{B}_i$ is the 3×3 symmetric matrix describing the ellipsoid's shape, i.e. at the vortex boundary $(\boldsymbol{x} - \boldsymbol{X}_i)^T\mathscr{B}_i^{-1}(\boldsymbol{x} - \boldsymbol{X}_i) = 1$. The strength of a vortex i is κ_i, i.e. the volume integral of PV scaled by 4π. H is the Hamiltonian of the system, that is the total energy of the system scaled by 4π. Finally, $\mathscr{S}_i$ is the flow matrix of the locally linear velocity field at the boundary of the

Ratio	Range	Increment
q_1/q_2	0.4–2.2	0.2
V_1/V_2	0.1–1.0	0.1
$\Delta z/(h_1+h_2)$	0.005–0.75	0.25
h_1/r_1	0.6–1.2	0.2
h_2/r_2	0.6–1.2	0.2

TABLE 1. Range of the various parameters for the investigation of the equilibria (6400 parameter sets in total). A zero vertical offset is avoided by using $\Delta z/(h_1+h_2)=0.005$ instead, to exclude exactly symmetric conditions.

vortex i. $\mathscr{S}_i$ can be decomposed as $\mathscr{S}_i=\mathscr{S}_i^v+\mathscr{S}_i^b$ where $\mathscr{S}_i^v$ is the self-induced part and $\mathscr{S}_i^b$ is the part induced by all other ellipsoids in the flow. The self-induced flow is exactly linear at the boundary of the ellipsoid although this is only approximately true for the part induced by other ellipsoids. $\mathscr{S}_i^v$ is well known and can be evaluated in terms of elliptic integrals of the second kind.

For $\mathscr{S}_i^b$, we approximate it using 7 singularities (point vortices). The positions and strengths of the singularities are chosen so that the streamfunction they induce matches the exact ellipsoidal streamfunction to the order of accuracy $O(1/d^7)$, where d is the distance between the vortex centroid and the evaluation point. The singularities are used to compute the interaction energy and consequently the Hamiltonian H^b.

From this simplified Hamiltonian system, we can obtain equilibrium states (co-rotating vortices with fixed shape) and determine their linear stability (further details may be found in Reinaud & Dritschel 2005). The linear stability analysis identifies the conditions which precipitate a strong interaction. While this is important, we want to go further and examine the ensuing nonlinear interaction, in particular to determine the outcome. We focus on the marginally unstable equilibria as these are relevant to vortices drifting together, adiabatically, under the influence of vortices further afield (cf. Dritschel 1995; Legras, Dritschel & Caillol 2001; Scott & Dritschel 2006). To this end, we employ the contour-advective semi-lagrangian (CASL) algorithm which is ideally suited to modelling uniform-PV vortices with minimal numerical dissipation (Dritschel & Ambaum 1997). The initial conditions consist of marginally unstable ellipsoidal vortices as determine by the ELM. Note that the CASL algorithm simulates the full QG dynamics, hence includes non-ellipsoidal deformations (and much more). Nearly 400 simulations were performed to sample the 6400 sets of equilibria analysed.

3. The equilibrium states

3.1. *Geometry and basic properties of the equilibrium states*

The geometry of the flow is illustrated in figure 1. The vortices have a half-height h_i, volume V_i, mean horizontal radius r_i, and PV q_i ($i=1,2$). Hence, the vortex volume ratio is V_1/V_2, the vortex PV ratio is q_1/q_2, and the height-to-width aspect ratios are h_1/r_1 and h_2/r_2. We denote the relative vertical offset by $\Delta z/(h_1+h_2)$ and the horizontal gap by δ. In order to compare the different cases, the total volume of PV is set to $V_t=4\pi/3$ while the total strength (i.e. the volume integral of PV) is set to $S_t=8\pi^2/3$, corresponding to a mean PV of 2π. The range of parameter values considered is given in table 1. We focus on vortices having height-to-width aspect ratios h_i/r_i in the range 0.6 to 1.2, the range most commonly found in QG turbulence, based on CASL simulations (Reinaud *et al.* 2003). More oblate or prolate vortices are

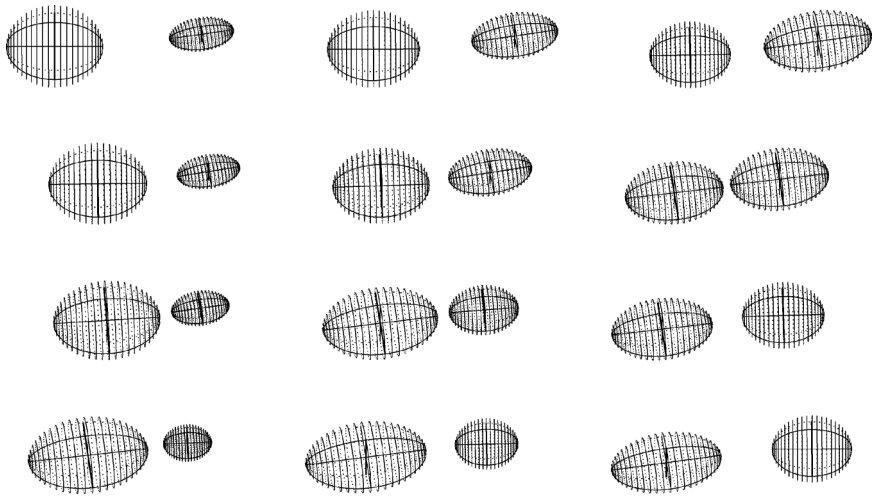

FIGURE 2. Equilibrium states at the margin of stability for $h_1/r_1 = h_2/r_2 = 0.8$, and $\Delta z/(h_1 + h_2) = 0.5$. The first column corresponds to $V1/V_2 = 0.1$, the second to $V1/V_2 = 0.3$, and the third to $V1/V_2 = 1.0$. The first row corresponds to $q_1/q_2 = 0.4$, the second to $q_1/q_2 = 1$, the third to $q_1/q_2 = 2$ and the fourth to $q_1/q_2 = 4$.

rarely found in QG turbulence; the most common aspect ratio is approximately 0.8. Although other vortex aspect ratios may be found say in the real ocean, we believe they are relatively rare and do not consider them here.

For illustration, we have also computed equilibria for vortices having a PV ratio larger than 2.2. Figure 2 shows selected equilibria at the margin of stability for $h_1/r_1 = h_2/r_2 = 0.8$, $\Delta z/(h_1 + h_2) = 0.5$, $V_1/V_2 = 0.1$, 0.3, 1 (left to right), and $q_1/q_2 = 0.4$, 1, 2, 4 (top to bottom) to illustrate the combined effects of the PV ratio and the volume ratio. As expected, increasing the strength of one vortex $q_i V_i$ results in its being less deformed (i.e. more spheroidal). On the other hand, weak vortices are strongly deformed by the strain induced by the stronger vortex. It is also noticeable from the figure that the margin of stability appears to correspond to smaller separation distances when the PV ratio q_1/q_2 is around 1 or 2. Figure 3 shows another selection of equilibria at the margin of stability. Here, we take $h_1/r_1 = h_2/r_2 = 0.8$, $V_1/V_2 = 0.3$, and $\Delta z/(h_1 + h_2) = 0.005$, 0.25, 0.75 (left to right), and $q_1/q_2 = 0.4$, 1, 2 and 4 (top to bottom) to illustrate the combined effects of the PV ratio and vertical offset. Increasing the vertical offset increases the angle with which the vortices tilt toward each other. However, we see that the tilt angle of a vortex decreases as its strength increases. Again, we observe that the margin of stability corresponds to smaller separation distances when the PV ratio q_1/q_2 is around 1 or 2.

The procedure to determine families of equilibria is the same as that used in Reinaud & Dritschel (2005). For each family of equilibrium states, i.e. given values of the aspect ratios, volume ratio, PV ratio and vertical offset, we start with two spheroidal vortices well separated in the horizontal. Fixing the horizontal gap δ between the two vortices, we start the iterative procedure to converge toward the equilibrium state. Once the equilibrium state is found, the horizontal gap δ is reduced by a small amount (2×10^{-4}) and the iterative procedure is resumed for the next state. We continue just past the point of maximum energy $-\frac{1}{2}\iiint q\psi \mathrm{d}V$, which in all cases coincides with the margin of stability (see below as well as Reinaud & Dritschel (2005) for further remarks and analogies to the two-dimensional problem).

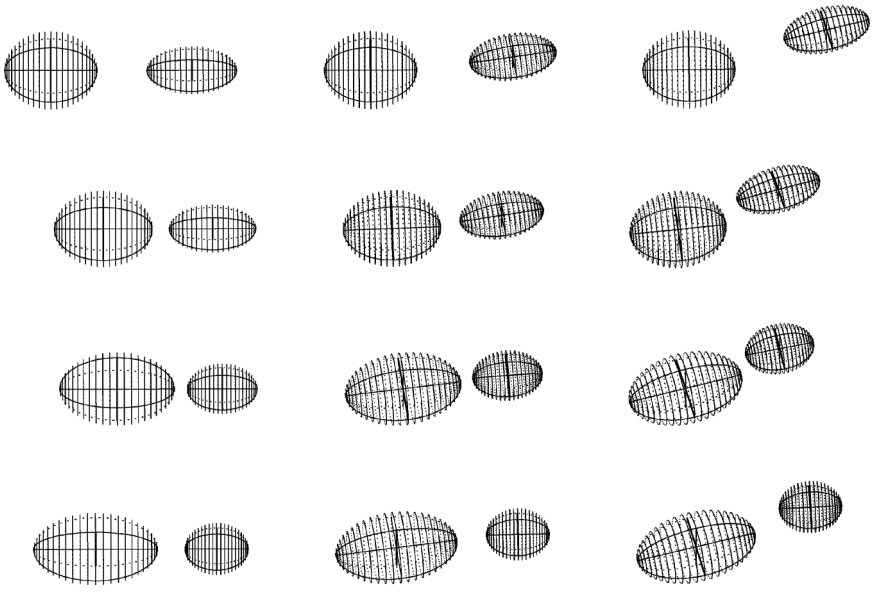

FIGURE 3. Equilibrium states at the margin of stability for $h_1/r_1 = h_2/r_2 = 0.8$, and $V_1/V_2 = 0.3$. The first column corresponds to $\Delta z/(h_1+h_2) = 0.005$, the second to $\Delta z/(h_1+h_2) = 0.25$, and the third to $\Delta z/(h_1+h_2) = 0.75$. The first row corresponds to $q_1/q_2 = 0.4$, the second to $q_1/q_2 = 1$, the third to $q_1/q_2 = 2$ and the fourth to $q_1/q_2 = 4$.

3.2. *Linear stability*

The scheme used to calculate the linear stability of general vortex equilibrium is detailed in Reinaud & Dritschel (2005). Here we apply the simplified ellipsoidal stability analysis based on the ELM. In this analysis, only ellipsoidal disturbances are considered by construction. Nonetheless, comparisons with a complete analysis based on the full QG equations in Reinaud & Dritschel (2005) indicate that this approximation is not restrictive, as the first unstable mode is consistent with an ellipsoidal mode. The same conclusion was reached by McKiver & Dritschel (2006) for single ellipsoids in a linear background shear.

A typical example of the ELM linear stability analysis is shown in figure 4, focusing on the range of δ near marginal stability. In all cases, two modes with frequencies $\pm\sigma_i$ merge at $\delta = \delta_c$ when decreasing δ. For $\delta < \delta_c$, σ_i remains zero and now there is a pair of modes with growth rates $\pm\sigma_r$, one stable, the other unstable. This 'exchange type' instability appears to be generic, as it has been found in numerous stability analyses of vortex pairs, both in two-dimensional and three-dimensional QG dynamics (cf. Dritschel 1995; Reinaud & Dritschel, 2005 and references therein). In all cases, instability erupts at the maximum of the energy E of the vortex system. This instability triggers a strong interaction between the two vortices during their nonlinear evolution (see below).

We now examine the distance between the centroids of the two vortices $\delta_{3D} = |\boldsymbol{X}_1 - \boldsymbol{X}_2|$ below which instability occurs, in the complete parameter space. Here, for brevity, we illustrate only a small part of the parameter space in figures 5 and 6, for $\Delta z/(h_1 + h_2) = 0.005$ and 0.75, respectively (additional material is available with the online version of the paper). Each plot shows δ_{3D} as a function of V_1/V_2 and q_1/q_2, for two values of each aspect ratio, $h_i/r_i = 0.6$ and 1.2. In a few cases (indicated by triangles), the margin of stability could not be reached by the iterative method

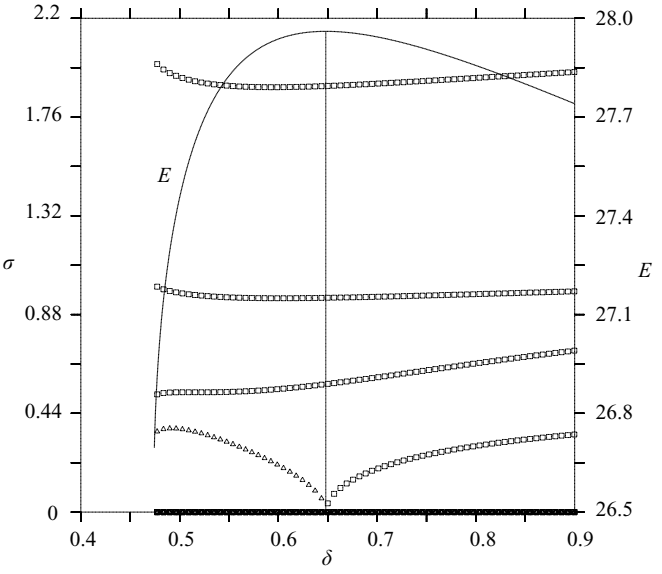

FIGURE 4. The (positive) mode growth rates σ_r (□) and frequencies σ_i (△) obtained from the linear stability analysis plotted versus the gap δ for $q_1/q_2 = 2$, $h_1/r_1 = h_2/r_2 = 1$, $V_1/V_2 = 1$, and $\Delta z/(h_1 + h_2) = 0.25$. Only every 32nd data point is plotted for clarity. Altogether, there are 4 pairs of modes with either opposite σ_r and zero σ_i, or opposite σ_i and zero σ_r. The curve corresponds to the energy and the vertical line indicates the location of the margin of stability, which coincides with the maximum of energy.

employed. This happens when the vertical offset is small and at least one of the vortices exhibits a near-circular cross-section. Similar difficulties were found in Reinaud & Dritschel (2005) and attributed to a spurious oscillating numerical mode arising from the discrete representation used to model the external flow induced by the ellipsoids. When the margin of stability could not be reached, we extrapolated δ_{3D} quadratically using the known data at vertical offsets $\Delta z/(h_1 + h_2) = 0.25$, 0.5 and 0.75. Three data points could not be obtained for $\Delta z/(h_1 + h_2) = 0.75$ for the same reasons, and are interpolated linearly from known data for different height-to-width aspect ratios.

We find that the smallest distances δ_{3D} occur for large PV ratios and small volume ratios (the upper left-hand corner of each contour plot). However, the trend observed suggests that the distance would increase for higher PV ratios. On the other hand, the largest distances occur for small values of both the PV ratio and the volume ratio (lower left-hand corner). Again, the observed trend suggests that large values for δ_{3D} would be obtained for large PV and volume ratios. A saddle of smaller distances extends from the upper left-hand corner down and across the centre of each plot. This saddle marks the parameter values for which two vortices are most robust, in the space of volume and PV ratios. The saddle is a valley of smaller distances, and when crossing the valley one reaches a minimum point corresponding to where the vortices are minimally separated and still just stable. The saddle is well correlated with $q_1/q_2 = 1/(V_1/V_2)$ or $q_1V_1 = q_2V_2$. This is the condition of equal vortex strengths. Hence vortices of equal strength are most stable, over all strength ratios, for fixed vertical offsets and aspect ratios. We also recover the result initially obtained for equal PV vortices in Reinaud & Dritschel (2002, 2005), namely that vortices moderately offset in the vertical are likely to interact strongly from larger separation distances. In other words, for a fixed horizontal separation, a moderate vertical offset is destabilizing.

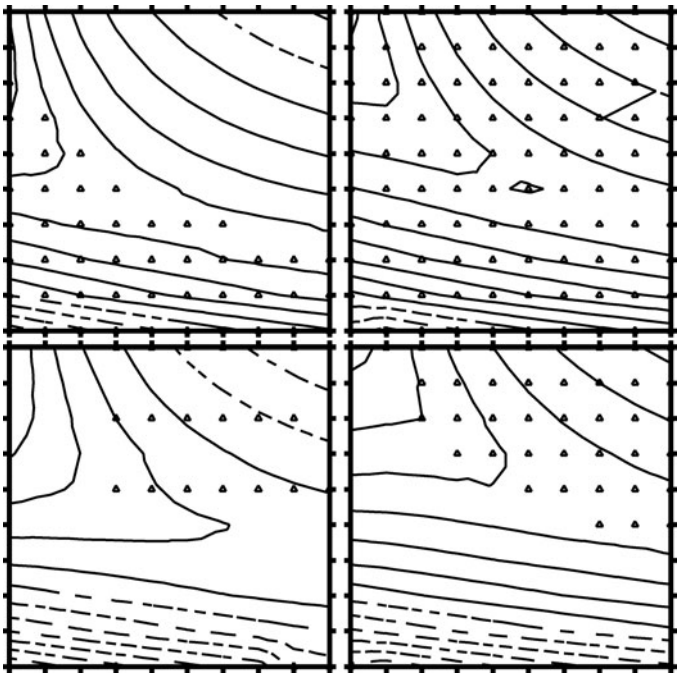

FIGURE 5. Iso-levels of the vortex separation δ_{3D} at the margin of stability for $\Delta z = 0.005(h_1 + h_2)$. The x-axis of each contour plot corresponds to the volume ratio, $0.1 < V_1/V_2 < 1.0$, while the y-axis corresponds to the PV ratio, $0.4 < q_1/q_2 < 2.2$. The left-hand two figures are for $h_1/r_1 = 0.6$ and the right-hand two figures are for $h_1/r_1 = 1.2$, whereas the bottom two figures are for $h_2/r_2 = 0.6$ and the top two figures are for $h_2/r_2 = 1.2$. The first solid contour is for $\delta_{3D} = 2.605$. Larger values are indicated by dashed lines. The contour interval is 0.01. The small triangles mark points where data had to be extrapolated.

This counter intuitive results can be explained by the differences between horizontal strain and vertical shear, the latter being more destabilizing. Also note that the critical separation distance tends to increase as the aspect ratios decreases (the values of δ_{3D} are greatest in the lower left-hand corner contour plot in each array). This means that oblate vortices with $h_i/r_i < 1$ are generally less stable than prolate vortices, all other things being equal. This difference, however, becomes less significant as the vertical offset increases. Presumably, prolate vortices are then strongly affected by vertical shear.

We summarize the overall influence of the PV ratio by averaging δ_{3D} over the different volume ratios, height-to-width aspect ratios and vertical offsets. Figure 7 shows how this averaged distance $\bar{\delta}_{3D}$ varies with q_1/q_2. The averaged distance $\bar{\delta}_{3D}$ exhibits a smooth trend and reaches a minimum over the range $1.2 < q_1/q_2 < 1.4$, which, given the uncertainty in the data, implies that a minimum occurs for a PV ratio of about 1. This indicates that vortices with a stronger PV contrast are less robust: they destabilize at larger separation distances. Hence, from this result one would expect a population of vortices, say in turbulence, to develop similar PV values by selectively destroying weaker vortices – a kind of 'natural selection' among vortices. This scenario is supported by the nonlinear simulation results presented in the next section. This justifies, *a posteriori*, the attention paid in the literature to equal-PV vortex interactions as the primary model for understanding decaying turbulence.

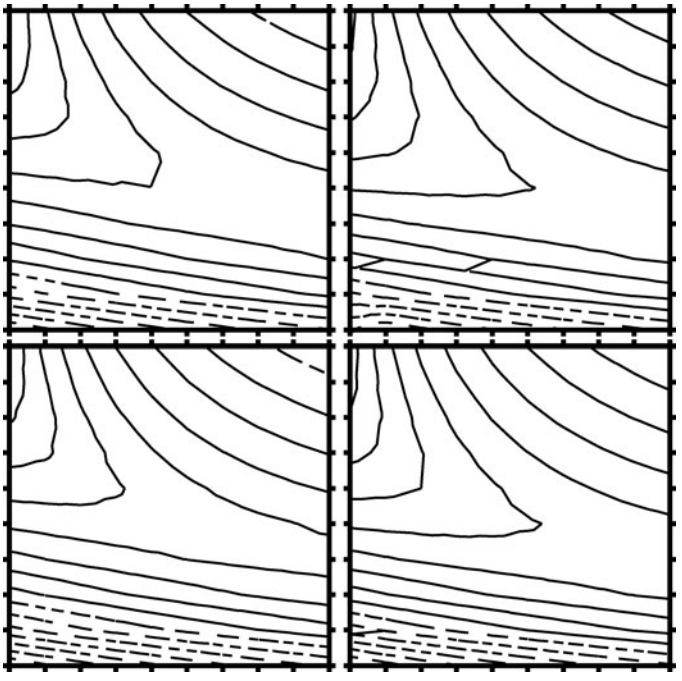

FIGURE 6. Iso-levels of δ_{3D} at the margin of stability for $\Delta z = 0.75(h_1 + h_2)$. See the caption of figure 5 for details. Here the first solid contour is for $\delta_{3D} = 2.685$.

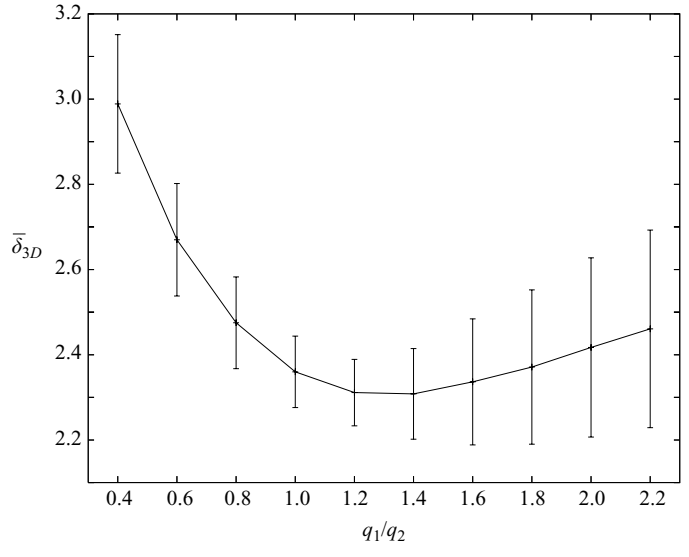

FIGURE 7. The mean value of the overall distance $\overline{\delta}_{3D}$ between the centroids of the two vortices at the margin of stability versus the PV ratio (averaged over V_1/V_2, h_1/r_1, h_2/r_2 and $\Delta z/(h_1 + h_2)$). The error-bars indicate ± 1 standard deviations.

4. Nonlinear interactions

4.1. *Numerical set-up*

In this section, we address the outcome of unstable interactions by solving the full QG equations using the CASL algorithm, introduced in Dritschel & Ambaum

(1997). The initial conditions for the nonlinear simulations consist of a pair of vortices at the margin of stability as determined in the previous section. Although these equilibria are not exact equilibria with respect to the full QG equations, they provide a good approximation of them (and moreover contain initial disturbances from the exact equilibrium to kick off the instability). The PV in the vortices is determined by ensuring that the total volume be $V_t = 4\pi/3$ and the total strength be $S_t = 8\pi^2/3$, as required of the equilibria described in the previous sections. The time step is $\Delta t = \pi/(10\, q_{max})$ where $q_{max} = max(q_1, q_2)$. The domain is triply periodic and of dimensions $(2\pi)^3$. To limit the effects of periodicity, the vortices are shrunk to fit into a 2^3-box at the centre of the computational domain, following Reinaud & Dritschel (2002). However, all diagnostics are computed for vortices scaled back to their original volumes. We use a 128^3 grid to invert the gridded PV and calculate the velocity field. PV contours are represented on four times as many isopycnal layers, and a grid four times finer in each horizontal direction is used in converting the PV contours to gridded PV values (this is standard). Contour surgery, which limits the growth in complexity of the contours, is applied at a twentieth of the horizontal grid resolution (see Dritschel & Viúdez 2003) for further standard numerical settings).

Simulations are run long enough for the final state to have reached a near equilibrium (i.e. when the volumes of the few largest vortices remain approximatively constant). Hence the final time may vary from one case to another. Typically, however, simulations are run for 60 time units, or 20 characteristic turn-around times based on the mean PV.

4.2. *Examples*

We first illustrate the nonlinear evolution in four cases. For each, we consider vortices having height-to-width aspect ratios $h_1/r_1 = h_2/r_2 = 0.8$, a volume ratio of $V_1/V_2 = 0.5$, and a vertical offset of $\Delta z/(h_1 + h_2) = 0.25$. Only the PV ratio differs between the cases. In the first case shown in figure 8, we take $q_1/q_2 = 0.6$, corresponding to a strength ratio of $q_1 V_1/q_2 V_2 = 0.3$. Here, the largest vortex (vortex 2) also has the largest PV. At $t = 0$, we see that in equilibrium (according to the ELM, that is), vortex 2 is less deformed (more spheroidal) than vortex 1. By $t = 9.5$, corresponding to 3.7 turn-around times $T = 6\pi/q_2 = 2.6$, a filament or tongue of PV is drawn from the weaker vortex 1 and begins to wrap around vortex 2, forming a thin spiral ring of PV which detaches from vortex 1 by $t = 15.5$. This spiral ring thins by differential rotation and is eventually removed by surgery. Vortex 2 is disturbed by the ring, but never changes volume – the vortices never merge, even partially. By the end of the simulation at $t = 57$, vortex 1 has lost 14.8 % of its volume. We may say that vortex 1 has been partially strained out during the interaction.

In the second example, presented in figure 9, we take $q_1/q_2 = 1$, hence the strength ratio is $q_1 V_1/q_2 V_2 = 0.5$. The two vortices merge at $t = 3.1$, a little more than 1 turn-around time $T = 6\pi/q_2 = 3$, forming a dumbbell-like vortex. This persists until $t = 11$, when it splits into two vortices and generates filamentary debris. After splitting, the original smaller vortex 1 loses 18.7 % of its original volume while the large vortex 2 gains 8.6 % in volume. About 0.4 % of the total volume has been lost to filaments. The vortices briefly merge, or rather touch again at $t = 16$, then split almost immediately, generating a tiny amount (< 0.1 %) of debris. After this time, the vortices no longer strongly interact, and thereafter shed only a small amount of filamentary debris. By the end of the simulation ($t = 57$), vortex 1 is now only 3.3 % larger than initially while vortex 2 is 20.5 % smaller. In this case, we may say that the vortices have partially merged.

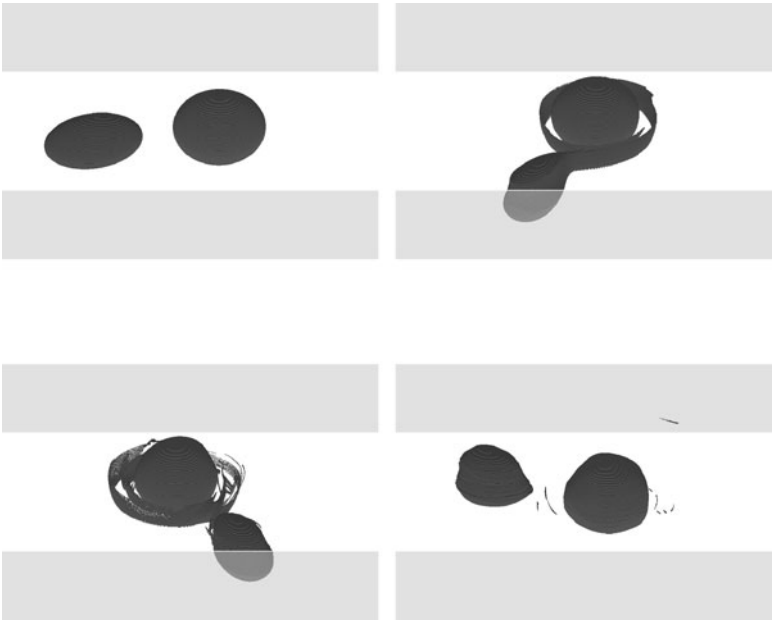

FIGURE 8. $q_1/q_2 = 0.6$, $h_1/r_1 = h_2/r_2 = 0.8$, $V_1/V_2 = 0.5$, $\Delta z/(h_1 + h_2) = 0.25$. Times displayed (left to right, then top to bottom) are $t = 0$, 9.5, 19 and 57. The view angle is 60° from the vertical in this and subsequent figures. The light-grey shaded areas show the back and front walls of the domain, over the range of layers spanned by the vortices.

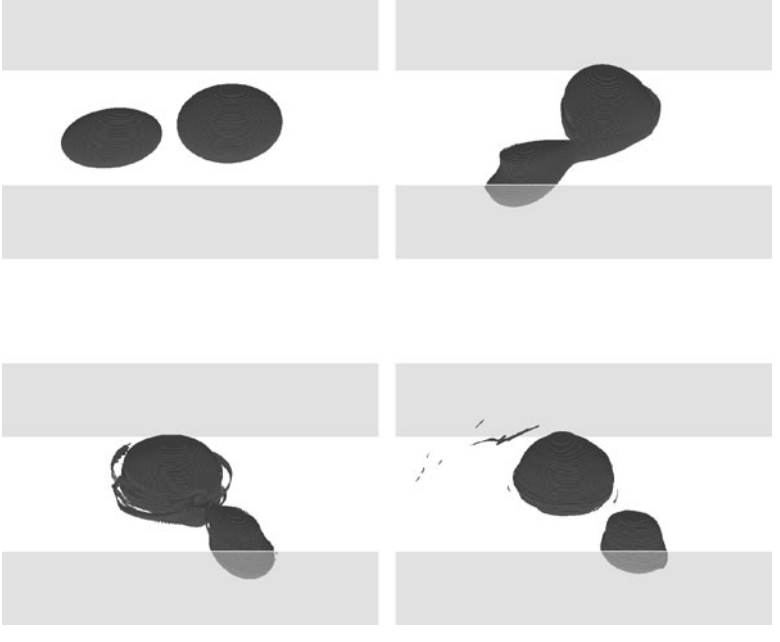

FIGURE 9. $q_1/q_2 = 1$, $h_1/r_1 = h_2/r_2 = 0.8$, $V_1/V_2 = 0.5$, $\Delta z/(h_1+h_2) = 0.25$. Times displayed (left to right, then top to bottom) are $t = 0$, 5, 12.9 and 57. See caption of figure 8 for more details.

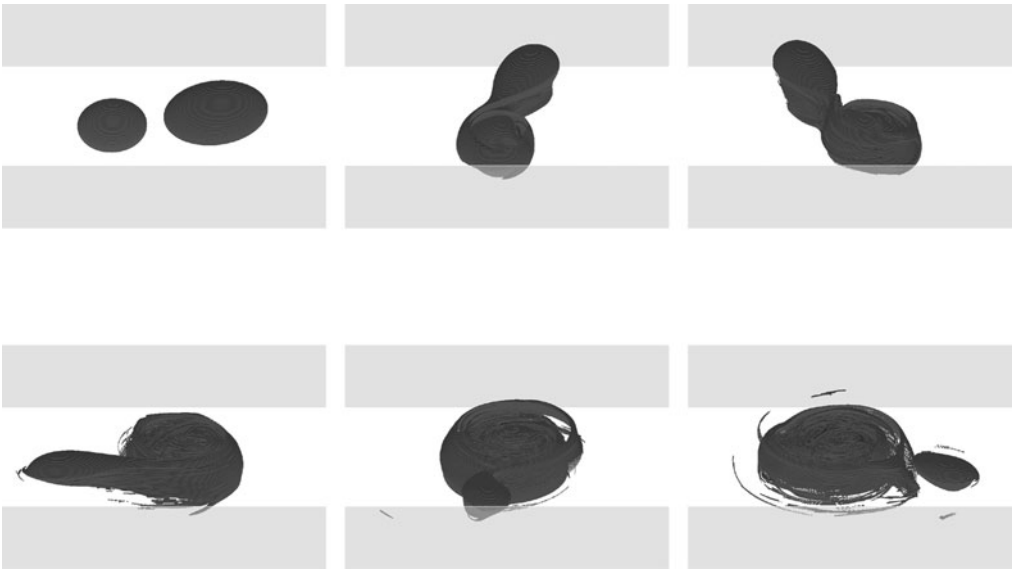

FIGURE 10. $q_1/q_2 = 2$, $h_1/r_1 = h_2/r_2 = 0.8$, $V_1/V_2 = 0.5$, $\Delta z/(h_1 + h_2) = 0.25$. Times displayed (left to right, then top to bottom) are $t = 0$, 8.1, 14.1, 26.7, 38, and 57. See caption of figure 8 for more details.

In the third example, presented in figure 10, we take $q_1/q_2 = 2$, hence the strength ratio is $q_1 V_1/q_2 V_2 = 1$. In this case, the smaller vortex 1 has the larger PV, but both vortices have identical strength. Initially, vortex 1 is less deformed than vortex 2. The two vortices merge into a single structure at $t = 7.4$, corresponding to 3.7 turn-around times $T = 6\pi/q_1 = 2$, with the lower-PV vortex being stretched into a large spiral ring encircling the high-PV vortex. Here the largest vortex is most strongly deformed. Most of it ends up in the spiral ring. Part of this ring remains loosely connected to the high-PV core belonging to vortex 1 initially. The ring forms a shield of lower PV around the core. This vortex-ring compound structure by $t = 43.2$ contains 76.6 % of the total initial volume of PV, while the secondary vortex contains 16.5 % of the total initial volume. The remainder consists of filaments. From this time, until the end of the simulation at $t = 57$, the vortices no longer strongly interact. The secondary vortex remains mostly unchanged, whereas the larger compound vortex is gradually eroded at its periphery. By $t = 57$, it has lost 9.61 % of the volume it had at $t = 43.2$. We may again consider this case a partial merger.

Finally, we illustrate in figure 11 an example of an interaction for a PV ratio of 4, a higher PV ratio than those considered in § 3.1, simply for contrast. The vortex strength ratio is here $q_1 V_1/q_2 V_2 = 2$. The small intense vortex 1 on the left is little deformed initially from a spheroid. In time, vortex 1 draws out a thin filament from vortex 2 which forms a spiral ring around vortex 1: this is reminiscent of the first case in figure 8, with vortices reversed. Little debris are generated. The ring finally detaches from the low-PV vortex 2 at $t = 45.6$. This ring contains 22.5 % of the initial volume of vortex 2, which remains the largest vortex of the flow with 72.7 % of its original volume by the end of the simulation at $t = 57$. The remaining volume consists of filamentary debris. We may call this case a partial straining out of the large vortex.

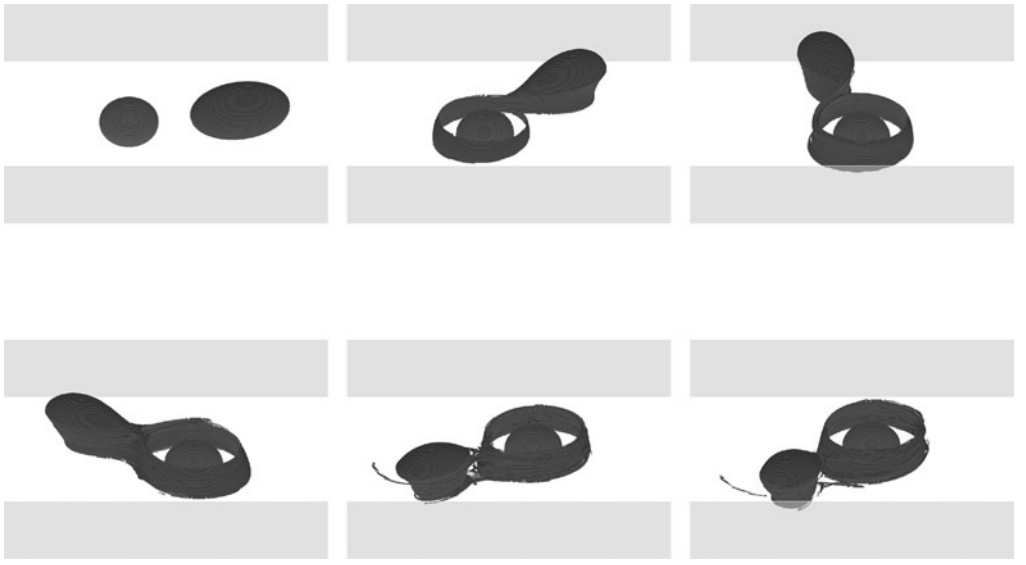

FIGURE 11. $q_1/q_2 = 4$, $h_1/r_1 = h_2/r_2 = 0.8$, $V_1/V_2 = 0.5$, $\Delta z/(h_1 + h_2) = 0.25$. Times displayed (left to right, then top to bottom) are $t = 0$, 8.6, 21, 30.6, 43.4, and 46.6. See caption of figure 8 for more details.

Parameter	Range
q_1/q_2	$\{0.6, 0.8, 1.0, 1.2, 1.6, 2.0, 3.0, 4.0\}$
V_1/V_2	$\{0.1, 0.5, 1.0\}$
$\Delta z/(h_1 + h_2)$	$\{0.005, 0.25, 0.5, 0.75\}$
$(h_1/r_1, h_2/r_2)$	$\{(0, 6, 1, 2), (0.8, 0.8), (1.0, 1.0), (1.2, 0.6)\}$

TABLE 2. Parameters used in the initial conditions for the numerical simulations.

4.3. *Classification of vortex interactions*

We next examine the general characteristics of vortex interactions across the entire parameter space. We cannot consider all 6400 cases considered in § 3.1, owing to computational expense, and therefore restrict attention to a broad subset of cases. Our main interest in this study is the influence of the PV ratio q_1/q_2 on vortex interactions, so we consider a wide variety of values of this parameter (see table 2). The main restriction on the sampling of the other parameters is on the height-to-width aspect ratios: we limit the choice for h_1/r_1 and h_2/r_2 to 4 pairs of values. We also consider 3 values for the volume ratio V_1/V_2 and 4 values for the vertical offset – see table 2. Note that we include a few cases with PV ratios higher than in § 3.1. Altogether, this subset includes 384 individual cases. However, in 22 cases we could not determine the marginally unstable equilibria, hence could not generate an appropriate initial condition for a numerical simulation. These cases correspond to vortices nearly aligned in the vertical, as discussed in § 3.2. Considering the number of cases which could be examined, these few exceptions are unlikely to affect the general conclusions.

Our principal aim is to classify the different types of interactions occurring. We use a classification similar to that proposed for two-dimensional vortex interactions by Dritschel & Waugh (1992) and used in three-dimensional vortex interactions by

Interaction type	$\hat{V}_f$	$\hat{V}_s$
Elastic interaction (EI)	1	1
Partial straining out (PSO)	$\leqslant 1$	< 1
Complete straining out (CSO)	$\leqslant 1$	0
Partial merger type 1 (PM1)	>1	< 1
Partial merger type 2 (PM2)	<1	>1
Complete merger (CM)	>1	0

TABLE 3. Classification of vortex interactions.

Bambrey *et al.* (2007). We define $\hat{V}_f$ as the ratio of the volume of the largest vortex in the flow by the end of the simulation to the volume of the largest vortex at $t=0$. Similarly, we define $\hat{V}_s$ as the ratio of the volume of the second largest vortex in the flow by the end of the simulation to the volume of the second largest vortex at $t=0$. Depending on the value of $\hat{V}_f$ and $\hat{V}_s$, we classify the vortex interaction as outlined in table 3. The interactions fall into 6 types: (i) elastic interaction (EI) when vortices do not change volume; (ii) partial straining out (PSO) when a part of one or both vortices has been removed but does not lead to the growth of any of the vortices; (iii) complete straining out (CSO), when one vortex is completely destroyed by the straining field of the other but is not absorbed by it; (iv) partial merger type 1 (PM1), when the two vortices have exchanged PV, and when the largest vortex at the end of the interaction is larger than the largest vortex at $t=0$; (v) partial merger type 2 (PM2), when the vortex which gained volume is initially the second largest vortex but does not become larger than the largest vortex at $t=0$; and (vi) the complete merger (CM), when only one vortex, containing all of the coherent PV, survives the interaction. Departing from the classification used in Bambrey *et al.* (2007), we distinguish two types of partial merger (PM1, PM2). PM1 is the same as the one the authors used. For PM2, the second largest vortex 1 incorporates a part of the PV of the largest vortex 2, yet not enough to become the largest vortex of the flow by the end of the simulation. This is possible when initially the second largest vortex 1 has a higher PV than the largest vortex 2. For the equal-PV interactions considered in Bambrey *et al.* (2007), this situation cannot happen as the largest vortex 2 always dominates the interaction.

Overall, 21.7 % of all interactions investigated were found to be PSO, and 70.5 % PM1, and 7.8 % are PM2. No other type of interaction was observed. It is perhaps not surprising that we do not encounter EI as we start at the (estimated) margin of stability. Hence we expect a strong interaction to take place in all cases. On the other hand, the complete absence of CSO and CM interactions indicates that, in general, vortex interactions are hardly ever fully destructive (lack of CSO), and are rarely – if ever – complete merger (lack of CM). The notion of 'vortex merger' is even less appropriate in three-dimensions than it is in two-dimensions (Dritschel & Waugh 1992).

We now focus on the influence of the PV ratio on the types of interaction observed. Note that the sample size for each PV ratio is only about 45 simulations, so there may be significant uncertainty in the results reported next. The results are summarized in table 4. The first result is that, in the parameter space considered here (except for the PV ratio $q_1/q_2=3$), PM1 is the dominant interaction. In these cases, the largest vortex grows in volume as a result of the interaction. This indicates the possibility of an inverse energy cascade in physical space as larger more energetic vortices are

IT/PV ratio	0.6	0.8	1.0	1.2	1.6	2.0	3.0	4.0
PSO	11.1	17.8	28.3	8.7	22.2	24.4	46.5	22.2
PM1	88.9	82.2	71.7	91.3	75.6	68.9	32.6	40.0
PM2	0	0	0	0	2.2	6.7	20.9	37.8

TABLE 4. Percentages of PSO, PM1 and PM2 regimes for the 8 PV ratio considered. IT stands for Interaction type.

formed on average. Note that vortices have a self-energy roughly proportional to r^5, where $r = (3V/4\pi)^{1/3}$ is their mean radius, see Bambrey *et al.* (2007). The self-energy of a vortex is defined by

$$E = -\frac{1}{2}\int\int\int_V q\psi^v \mathrm{d}V, \tag{4.1}$$

where V denotes the volume occupied by the vortex, ψ^v is the streamfunction induced by the vortex, and q is its PV. We focus on the self-energy since this dominates the interaction energy, often by a factor of 10 or greater (see Reinaud & Dritschel 2005, in particular their figure 8). Moreover, as illustrated below, the self-energy allows us to assess, in a simple way, energy exchanges between spatial scales resulting from strong interactions.

When the PV ratio is larger than 1, the first cases of PM2 are observed. Note that since the volume ratio is set to be less than 1 (without loss of generality), when the PV ratio is less than 1, the largest vortex 2 also has the highest PV and dominates the interaction. In these cases, the smaller vortex 1 is never able to incorporate more PV than it loses. However, when the PV ratio is larger than 1, the smallest vortex 1 may dominate the interaction and incorporate some of the volume of the largest vortex 2 (as seen for example in figure 10). The percentage of PM2 increases as the PV ratio increases, which is expected as the increased PV of the smaller vortex 1 makes it more likely to dominate the interaction. In these PM2 interactions, the initially largest vortex 2 loses volume while the initially smallest vortex 1 gains volume. This favours the formation of intermediate-sized vortices rather than larger vortices. Recall, however, that these interactions occur at larger separation distances than in the case of similar-PV vortices. Hence, in a (freely-evolving) turbulent flow, interactions between dissimilar-PV vortices are likely to take place relatively early in the evolution, and therefore become rare at late times.

The present results also show that PSO interactions occur frequently. Bambrey *et al.* (2007) found that, for equal-PV vortices, this regime is typical when the vortex volume ratio is much smaller than 1. Here, over a wide range of PV ratios, this regime occurs in about 20 % of all cases, in particular when the vortex strengths are strongly dissimilar. The complexity of vortex interactions seen here underscores the fact that vortex interactions are much more complex than the classical 'vortex merger', originally thought to be the primary mechanism for energy cascades in geophysical turbulence.

4.4. *Volume, strength, energy and enstrophy*

In the previous section, we examined the changes in volume of the vortices as a result of their interaction. Such changes may be directly related to scale changes and hence to energy transfers in physical space. Most interactions result in the growth in volume of the largest vortex (PM1), supporting the notion of an inverse energy cascade for QG

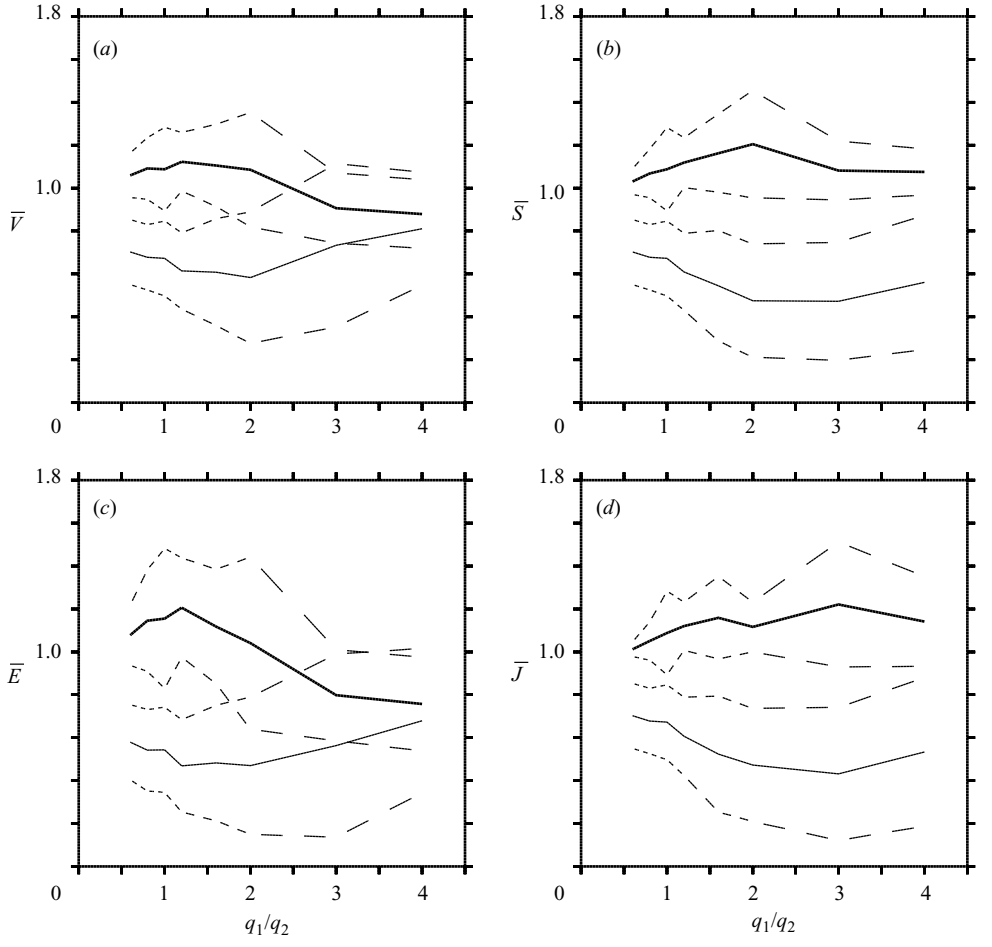

FIGURE 12. (*a*) Averaged volume ratios $\bar{V}_f$ (bold solid line) and $\bar{V}_s$ (thin solid line) *vs.* q_1/q_2. The bold (resp. thin) dashed lines indicates the averaged value $\pm$ one standard deviation for $\bar{V}_f$ (resp. $\bar{V}_s$). (*b*) Similar figure for $\bar{S}_f$ and $\bar{S}_s$. (*c*) Averaged energy ratios $\bar{E}_f$ and $\bar{E}_s$. (*d*) Averaged enstrophy ratios $\bar{J}_f$ and $\bar{J}_s$.

turbulence; but many interactions fall into the PSO and PM2 regimes, and for these $\hat{V}_f \leqslant 1$. There is, however, another viewpoint. The main dynamical quantity is not the volume but the strength of the vortices $S = \iiint_V q \mathrm{d}V$. It is therefore also important to study how the vortex strengths change during the interactions. Analogous to $\hat{V}_f$ and $\hat{V}_s$, we introduce $\hat{S}_f$ and $\hat{S}_s$, where $\hat{S}_f$ is the ratio of the largest vortex strength at the end of the simulation to the largest vortex strength at $t = 0$, and $\hat{S}_s$ is defined in a similar way for the second largest strength. Moreover, we introduce analogous quantities for the averaged energy $\hat{E}_f$ and $\hat{E}_s$, and enstrophy $\hat{J}_f$ and $\hat{J}_s$, in order to examine directly energy and enstrophy changes or 'cascades'.

The averaged volume ratios ($\bar{V}_f$, $\bar{V}_s$), strength ratios ($\bar{S}_f$, $\bar{S}_s$), energy ratios ($\bar{E}_f$, $\bar{E}_s$), and enstrophy ratios ($\bar{J}_f$, $\bar{J}_s$) versus the PV ratio q_1/q_2 are summarized in figures 12(*a*)–12(*d*), respectively. Both $\bar{V}_f$ and $\bar{E}_f$ exhibit a maximum for $q_1/q_2 = 1$, indicating that interactions between equal-PV vortices are the most efficient in generating both larger and more energetic vortices and in promoting the inverse energy cascade. On the

other hand, for PV ratios larger than 1, $\bar{V}_f$ decreases as q_1/q_2 increases; meanwhile, $\bar{V}_s$ increases but remains less than 1 for all PV ratios. Between $q_1/q_2 = 2$ and $q_1/q_2 = 3$, $\bar{V}_f$ becomes less than 1. This means that there is on average a decrease in volume of the largest vortex for large PV ratios. This is consistent with the classification of vortex interactions presented in the previous section where we observe a large number of PSO and PM2 interactions occurring for large PV ratios (see table 4). These interactions do not result in an increase in volume of the largest vortex. On the other hand, it is seen that $\bar{S}_f$ is always larger than 1. This indicates that interactions always produce a stronger vortex, even if it might not be the largest vortex in the flow. Note that $\bar{S}_s$ is always less than 1. This means that interactions also produce a weaker vortex. A similar statement can be made for $\bar{J}_f$. Vortex interactions tend to increase the enstrophy of one of the vortices.

It is perhaps surprising that $\bar{S}_f > 1$ although $\bar{V}_f < 1$ and $\bar{V}_s < 1$ for large PV ratios. A possible explanation for this is as follows. At $t = 0$, the smaller vortex 1 is the strongest vortex. During the subsequent interaction, vortex 1 incorporates part of the initially larger but weaker vortex 2. By the end of the simulation, the largest vortex consists of a core of high PV initially belonging to vortex 1, shielded by lower PV coming from vortex 2. The volume of PV incorporated by the strongest vortex increases its strength ($\hat{S}_f > 1$), and makes it the largest vortex in the flow by the end of the simulation. However, this increased volume may not be enough to make it larger than vortex 2 at $t = 0$ ($\bar{V}_f < 1$). Moreover vortex 2 may have lost enough volume to become smaller than vortex 1 at $t = 0$, hence $\hat{V}_s < 1$.

To summarize, interactions on average tend to produce a larger, more energetic vortex when the PV ratio $q_1/q_2 \lesssim 1$, and a smaller vortex (or intermediate-sized one) when $q_1/q_2 \gtrsim 1$. On the other hand, interactions always produce a stronger vortex. Overall, averaging $\bar{V}_f$ and $\bar{S}_f$ over all PV ratios q_1/q_2, the volume of the largest vortex increases by 6 % and the strength of the strongest vortex increases by 12 %.

5. Conclusions

In this study we have analysed the interactions between two co-rotating (like-signed) quasi-geostrophic vortices having different height-to-width aspect ratios, volume ratios, potential vorticity ratios and vertical offsets.

We have first determined the onset of a possible strong interaction between the two vortices using an asymptotic approach provided by the ellipsoidal model. The analysis enabled us to determine approximate equilibria and the margin of stability for families of vortices. The first important result is that, on average, vortices having a PV ratio close to 1 must be closer inorder to interact strongly than vortices having large or small PV ratios. This has a direct implication for vortex interactions in general. Vortices with significantly different PV (around a factor 2 or more) are likely to interact strongly from further away than vortices with comparable PV. Then, the low-PV vortices are likely to be absorbed or strained out by the high-PV vortices. The implication of this result, for say geophysical turbulence, is that one should mainly find vortices of comparable PV at late times (after those having relatively weak PV have been strained out).

We have examined the outcome of a wide variety of vortex interactions by direct numerical simulation of the full QG equations. This has revealed the predominance of partial merger, a type of interaction in which the strongest vortex gains strength (volume integrated PV). Overall, the strongest vortex gains 12 % in strength, on

average. On the other hand, these interactions do not all yield a growth in volume for the largest vortex. This is particularly true for interactions between two vortices with a PV ratio larger than 2. However, on average, the gain in volume for the largest vortex is 6 % over the range of cases studied. Hence, overall, the largest vortices grow slightly in volume and strength on average, consistent with an inverse energy cascade in QG turbulence. At the same time, many smaller (and weaker) structures are produced.

A further topic under investigation is the interaction between two opposite-signed vortices. Opposite-signed vortices cannot merge, of course, and their interactions have been thought to be benign (Miyazaki, Yamamoto & Fujishima 2003) However, preliminary results indicate that such interactions can produce smaller vortices efficiently. Another topic concerns the extension of these results to flows at finite Rossby and Froude numbers, i.e. beyond the QG regime. This changes the way cyclonic and anti-cyclonic vortices interact.

This work has been done with the support of the UK Engineering and Physical Sciences Research Council (Grant GR/T00986/01).

REFERENCES

Bambrey, R. R., Reinaud, J. N. & Dritschel, D. G. 2007 Strong interactions between two co-rotating quasi-geostrophic vortices. *J. Fluid Mech.* **592**, 117–133.

Dritschel, D. G. 1995 A general theory for two-dimensional vortex interactions. *J. Fluid Mech.* **293**, 269–303.

Dritschel, D. G. 2002 Vortex merger in rotating stratified flows. *J. Fluid Mech.* **455**, 83–101.

Dritschel, D. G. & Ambaum, M. H. P. 1997 A contour-advective semi-Lagrangian algorithm for the simulation of fine-scale conservative fields. *Q. J. R. Met. Soc.* **123**, 1097–1130.

Dritschel, D. G. & de la Torre Juárez, M. 1996 The instability and breakdown of tall columnar vortices in a quasi-geostrophic fluid. *J. Fluid Mech.* **328**, 129–160.

Dritschel, D. G. & Viúdez, I. A. 2003 A balanced approach to modelling rotating stably stratified geophysical flows. *J. Fluid Mech.* **488**, 123–150.

Dritschel, D. G. & Waugh, D. W. 1992 Quantification of the inelastic interaction of unequal vortices in two-dimensional vortex dynamics. *Phys. Fluids* A **4**(8), 1737–1744.

Dritschel, D. G., Reinaud, J. N. & McKiver, W. J. 2004 The quasi-geostrophic ellipsoidal model. *J. Fluid Mech.* **505**, 201–223.

Ebbesmeyer, C. C., Taft, B. A., McWilliams, J. C., Shen, C. Y., Riser, S. C., Rossby, H. T., Biscaye, P. E. & Östlund, H. G. 1986 Detection, structure and origin of extreme anomalies in a western Atlantic oceanographic section. *J. Phys. Oceanoger.* **16**, 591–612.

Garrett, C. 2000 The dynamic ocean. In *Perspectives in Fluid Mechanics* (ed. G. K. Batchelor, H. K. Moffatt & M. G. Worster), pp. 507–553 Cambridge University Press.

Gill, A. E. 1982 *Atmosphere–Ocean Dynamics*. Academic.

von Hardenberg, J., McWilliams, J. C., Provenzale, A., Shchpetkin, A. & Weiss, J. B. 2000 Vortex merging in quasi-geostrophic flows. *J. Fluid Mech.* **412**, 331–353.

Legras, B., Dritschel, D. & Caillol, P. 2001 The erosion of a distributed two-dimensional vortex in a background straining flow. *J. Fluid Mech.* **441**, 369–398.

McKiver, W. J. & Dritschel, D. G. 2003 The motion of a fluid ellipsoid in a general linear background flow. *J. Fluid Mech.* **474**, 147–173.

McKiver, W. J. & Dritschel, D. G. 2006 The stability of a quasi-geostrophic ellipsoidal vortex in a background shear flow. *J. Fluid Mech.* **560**, 1–17.

Meacham, S. P. 1992 Quasigeostrophic, ellipsoidal vortices in stratified fluid. *Dyn. Atmos. Oceans* **16**, 189–223.

Meacham, S. P., Pankratov, K. K., Shchepetkin, A. F. & Zhmur, V. V. 1994 The interaction of ellipsoidal vortices with background shear flows in a stratified fluid. *Dyn. Atmos. Oceans* **21**, 167–212.

Meacham, S. P., Morisson, P. J. & Flierl, G. R. 1997 Hamiltonian moment reduction for describing vortices in shear. *Phys. Fluids* **9**, 2310–2328.

Miyazaki, T., Furuichi, Y. & Takahashi, N. 2001 Quasigeostrophic spheroidal vortices vortex model. *J. Phys. Soc Japan* **70**, 1942–1953.

Miyazaki, T., Yamamoto, M. & Fujishima, S. 2003 Counter-rotating quasigeostrophic ellipsoidal vortex pair. *J. Phys. Soc Japan* **72**, 1942–1953.

Reinaud, J. N. & Dritschel, D. G. 2002 The merger of vertically offset quasi-geostrophic vortices. *J. Fluid Mech.* **469**, 287–315.

Reinaud, J. N. & Dritschel, D. G. 2005 The critical merger distance between two co-rotating quasi-geostrophic vortices. *J. Fluid Mech.* **522**, 357–381.

Reinaud, J. N., Dritschel, D. G. & Koudella, C. R. 2003 The shape of the vortices in quasi-geostrophic turbulence. *J. Fluid Mech.* **474**, 175–192.

Scott, R. & Dritschel, D. 2006 Vortex-vortex interactions in the winter stratosphere. *J. Atmos. Sci.* **63**, 726–740.